

Electrodeposited Nanoflakes of $\text{RuO}_x \cdot n\text{H}_2\text{O}$ on Three-dimensional Graphene for Flexible Supercapacitors

WANG Yuan^{1,2}, LIN Jie^{1,2}, CHANG Zheng¹, LIN Tian-Quan¹, QIAN Meng^{1,2}, HUANG Fu-Qiang^{1,3}

(1. State Key Laboratory of High Performance Ceramics and Superfine Microstructure, Shanghai Institute of Ceramics, Chinese Academy of Sciences, Shanghai 200050, China; 2. University of Chinese Academy of Sciences, Beijing 100049, China; 3. State Key Laboratory of Rare Earth Materials Chemistry and Applications and Beijing National Laboratory for Molecular Sciences, College of Chemistry and Molecular Engineering, Peking University, Beijing 100871, China)

Abstract: Flexible electricity storage devices with high areal capacitance were urgently demanded due to recent development of advanced portable electronics. In this work, a facile cathodic electrodeposition method was employed to anchor $\text{RuO}_x \cdot n\text{H}_2\text{O}$ on three-dimensional graphene frameworks to realize improved utilization efficiency of $\text{RuO}_x \cdot n\text{H}_2\text{O}$ and shortened diffusion/transport path for electrons and protons, without adhesives. A high areal capacitance of $3.78 \text{ F} \cdot \text{cm}^{-2}$ was achieved at $2 \text{ mV} \cdot \text{s}^{-1}$, which was attributed to the feasible electrolyte transport into the nano layered-structure of $\text{RuO}_x \cdot n\text{H}_2\text{O}$. Furthermore, all-solid-state flexible supercapacitors were prepared for practical application, achieving an energy density of $0.1 \text{ mWh} \cdot \text{cm}^{-2}$ and a power density of $2.4 \text{ mW} \cdot \text{cm}^{-2}$ at a current density of $10 \text{ mA} \cdot \text{cm}^{-2}$, which surpassed most state-of-the-art works.

Key words: nano- $\text{RuO}_x \cdot n\text{H}_2\text{O}$; electrochemical deposition; supercapacitors

Recently, all-solid-state flexible supercapacitors have attracted enormous attention because of the increasing need for energy storage in the area of wearable electronic devices^[1-2]. For wearable electronic devices, the available area of devices is limited. Therefore, the areal capacitance is critical criteria for practical use. At present, the reported areal capacitance of supercapacitors ranges typically from $0.4 \text{ mF} \cdot \text{cm}^{-2}$ to $3 \text{ F} \cdot \text{cm}^{-2}$ ^[1, 3-8]. Thus, their practical applications^[9] of the supercapacitor are significantly limited by such a low value.

One of the most effective approaches to tackle the problem mentioned above is the utilization of pseudocapacitive materials, mainly transition metal oxides (RuO_2 ^[10], IrO_2 ^[11], Mn_3O_4 ^[12], and NiO_x ^[13]). Among various transition metal oxides, $\text{RuO}_x \cdot n\text{H}_2\text{O}$ is a promising candidate for supercapacitors due to its high electronic conductivity, long cycle life and high specific capacitance derived from their multiple oxidation states^[14-15]. However, the disadvantages of high expense and toxicity limit its extensive application. In this work, a small amount of $\text{RuO}_x \cdot n\text{H}_2\text{O}$ was deposited on three-dimensional graphene (3D-GR) frameworks at a mass loading of about 10 mg/cm^2 . In addition, most of these kinds of

electrode materials are in powder form, requiring insulating polymer binders (like polytetrafluoroethylene, polyvinylidene fluoride) to fabricate working electrodes, which hinder both the electron transport from $\text{RuO}_x \cdot n\text{H}_2\text{O}$ to current collectors and the ion transport between electrode and electrolyte^[16]. To address this issue, many transition metal oxides were anchored directly onto bulk substrates such as aligned carbon nanotube^[17], 3D nickel foam^[18], indium doped tin oxide (ITO)^[19], and carbon paper^[20]. Among various substrates, 3D-GR frameworks have many advantages when they are utilized as conductive scaffolds to deposit $\text{RuO}_x \cdot n\text{H}_2\text{O}$. The connected graphene networks can provide excellent electron transport paths, and its hierarchical porous structure can facilitate ions transport to the inner part of active materials^[21-23]. Another advantage is its hierarchical porous structure which can also work as template to grow porous and layered $\text{RuO}_x \cdot n\text{H}_2\text{O}$. Recently, Sun, *et al*^[21] used three-dimensional holey-graphene to load active materials niobia, showing ultrahigh-rate energy storage, proving 3D-GR is an excellent substrate for supercapacitors.

In this work, a cathodic electrodeposition method was

Received date: 2018-10-16; **Modified date:** 2018-12-04

Foundation item: National Key Research and Development Program (2016YFB0901600); Science and Technology Commission of Shanghai (16JC1401700, 16ZR1440500); National Natural Science Foundation of China (51672301); The Key Research Program of Chinese Academy of Sciences (QYZDJ-SSW-JSC013, KGZD-EW-T06); CAS Center for Excellence in Superconducting Electronics, and Youth Innovation Promotion Association CAS

Biography: WANG Yuan (1991–), male, candidate of PhD. E-mail: wangyuan@student.sic.ac.cn

Corresponding author: HUANG Fu-Qiang, professor. E-mail: huangfq@mail.sic.ac.cn

used to anchor nano- $\text{RuO}_x \cdot n\text{H}_2\text{O}$ on 3D-GR frameworks to realize improved utilization efficiency of $\text{RuO}_x \cdot n\text{H}_2\text{O}$ and shorten diffusion/transport path for electrons and protons. This cathodic electrodeposition method was proved to be an effective method to prepare nano metal oxides. Besides, 3D-GR frameworks were proved to be an excellent substrate for deposition. Moreover, all-solid-state flexible supercapacitor with a high areal capacitance of $1.02 \text{ F} \cdot \text{cm}^{-2}$ was achieved for practical application especially in which per-area performance is critical.

1 Experimental

1.1 Sample preparation

1.1.1 Preparation of $\text{RuO}_x \cdot n\text{H}_2\text{O}/3\text{D-GR}$

Chemical vapor deposition (CVD) was used to synthesize the porous few-layer carbon with porous Ni networks as templates^[24]. First, the porous Ni templates were ultrasonically cleaned for 30 min in the solution of acetic acid, alcohol, acetone and deionized water, separately. Second, the cleaned and dried porous Ni templates were put into a tube furnace at the atmosphere of CH_4 (20 sccm), H_2 (50 sccm) and Ar (300 sccm), heating to 1050°C for 100 min. Third, the samples were placed in 3 mol/L HCl solution for 72 h to completely dissolve Ni template. Finally, the samples were cleaned with deionized water and dried in the oven at 80°C for 4 h.

The cathodic electrodeposition was performed at electrochemical workstation (CHI760E, CH Instruments) using a three-electrode system with Ag/AgCl (KCl saturated) electrode as reference electrode and Pt wire as counter electrode. The conditions for deposition were -2 V , 5000 s. The aqueous electrolyte used in deposition was 5 mmol/L $\text{RuCl}_3 \cdot \text{H}_2\text{O}$, 0.02 mol/L HCl and 0.2 mol/L KCl. After deposition, the samples were annealed in the oven at 120°C for 12 h.

1.1.2 Preparation of all-solid-state flexible supercapacitors

For practical application, $\text{RuO}_x \cdot n\text{H}_2\text{O}/3\text{D-GR}$ combined with flexible carbon paper (0.1 mm) and gel polymer electrolyte were assembled to make all-solid-state flexible supercapacitors. 8 g polyvinyl alcohol was dissolved into 60 mL H_2SO_4 (2 mol/L) to form homogeneous mixtures under continuous stirring at 80°C for 2 h. Finally, the viscous mixture was poured into a glass petri dish and put in the fume hood at room temperature for several hours to vaporize the excess water. All-solid-state flexible supercapacitors were fabricated by sandwiching the polymer electrolyte between two electrodes.

1.2 Characterization

Field emission scanning electron microscopy (FE-SEM, Hitachi SU8200), transmission electron microscopy

(TEM, JEOL JEM-2100F) with an energy dispersive spectrometer (Oxford) and X-ray photoelectron spectroscopy (XPS, PHI 5000C ESCA System) (PerkinElmer) with Mg K α X-ray ($h\nu=1253.6 \text{ eV}$) at 14 kV were used to investigate the microstructure and composition of the samples.

A series of cyclic voltammetry (CV), galvanostatic charge/discharge (GCD) and A.C. impedance (EIS) tests, were performed on the electrochemical working station (CHI760E, CH Instruments). Three-electrode test system was conducted with Pt wire as counter electrode and Ag/AgCl (KCl saturated) electrode as reference electrode in the electrolyte of 1 mol/L H_2SO_4 . Two-electrode test system was used to test the electrochemical performance of all-solid-state flexible supercapacitors. EIS was performed from 0.01 Hz to 100 kHz at open circuit potential with an amplitude of 5 mV using three-electrode systems.

2 Results and discussion

The reaction process was illustrated in Fig. 1. When a negative potential of -2 V was applied, both H^+ and Ru^{3+} moved towards the working electrode. H^+ was reduced to H_2 , while parts of Ru^{3+} combined with OH^- to form $\text{RuO}_x \cdot n\text{H}_2\text{O}$ and the others was reduced to Ru. The *in-situ* generated hydrogen gas can act as the dynamic pore-forming template to create hierarchically porous structure of $\text{RuO}_x \cdot n\text{H}_2\text{O}$.

The morphology of 3D-GR was presented in Fig. 2(a) and the interlayer spacing of graphene was 0.34 nm as shown in Fig. 2(c). The field emission scanning electron microscopy (FE-SEM) images of $\text{RuO}_x \cdot n\text{H}_2\text{O}$ (Fig. 2(b)) showed that the $\text{RuO}_x \cdot n\text{H}_2\text{O}$ possessed layered structures, each of which was made of small particles signed by red circles whose diameter was about 2 nm, corresponding to the high-resolution transmission electron microscopy (HRTEM) images in Fig. 2(c). The stack of these particles

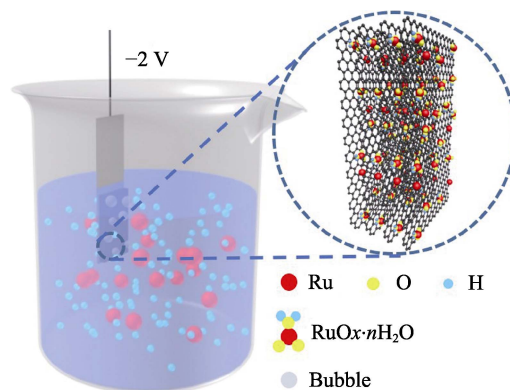


Fig. 1 Schematic of the reaction process and $\text{RuO}_x \cdot n\text{H}_2\text{O}/3\text{D-GR}$ configuration

formed a lot of pores and interconnected paths, which could facilitate electrolyte to access the inner part of the $\text{RuO}_x \cdot n\text{H}_2\text{O}$. The TEM images of $\text{RuO}_x \cdot n\text{H}_2\text{O}$ (Fig. 2(d-e)) were in broad agreement with FE-SEM results, indicating a layered structure of $\text{RuO}_x \cdot n\text{H}_2\text{O}$, and EDS elemental mapping (Fig. 2(f)) showed that the $\text{RuO}_x \cdot n\text{H}_2\text{O}$ particles were dispersed nearly homogeneously.

Three-electrode test systems were conducted to evaluate the electrochemical performance of the $\text{RuO}_x \cdot n\text{H}_2\text{O}/3\text{D-GR}$. Areal capacitance was calculated based on the equation (1) from CV curves:

$$C_s = S_{\text{area}} / (2v \cdot \Delta V \cdot S) \quad (1)$$

where S_{area} was the integrated area of current i and potential V in CV curves, v was the scan rate, ΔV was the potential window, and S was the area of working electrode.

GCD experiments were performed at different current densities to further investigate the electrochemical performance of $\text{RuO}_x \cdot n\text{H}_2\text{O}/3\text{D-GR}$. In GCD test, the areal capacitance was calculated by equation (2):

$$C_s = It / (\Delta V \cdot S) \quad (2)$$

where I was a set constant current and t was the discharge time, ΔV was the working voltage, and S was the area of the working electrode.

The correlation between the areal capacitance and the current densities was presented in Fig. 3(d). Remarkably, the areal capacitance of $\text{RuO}_x \cdot n\text{H}_2\text{O}/3\text{D-GR}$ reached a high value of $3.14 \text{ F} \cdot \text{cm}^{-2}$ even at a current density of $40 \text{ mA} \cdot \text{cm}^{-2}$, maintaining 75.0% of capacitance at $1 \text{ mA} \cdot \text{cm}^{-2}$, indicating excellent rate capability.

Long cycling stability, a crucial parameter for supercapacitors, was investigated by CV test at $10 \text{ mV} \cdot \text{s}^{-1}$ to determine the cycle life of $\text{RuO}_x \cdot n\text{H}_2\text{O}/3\text{D-GR}$. As shown in Fig. 4(b), the areal capacitance in the first cycle was $3.21 \text{ F} \cdot \text{cm}^{-2}$, and retained 86.9% ($2.79 \text{ F} \cdot \text{cm}^{-2}$) after 2×10^4 cycles, indicating excellent electrochemical stability.

According to the work done by Ferris, *et al*^[11], total capacitance (C_{outer}) and outer capacitance (C_{total}) were also employed to investigate the accessibility of charges by calculating the areal capacitances (C) as a function of the sweep rates (v). As demonstrated by Trasatti group^[25], C_{outer} meant the outer more accessible areal capacitances and C_{total} meant the total areal capacitances. In Lin, *et al*'s work^[26], C_{outer} was recognized as a rate-independent component k_1 (classically attributed to electrical double layer capacitance), taking the form^[25] (3)

$$C = k_1 + k_2 v^{-1/2} \quad (3)$$

which agreed with Ferris's work. The value of C_{outer} was acquired from the extrapolation of C to $v = \infty$, which extrapolate to $v^{-1/2} = 0$ intercept (Fig. 4(b)), whereas the total charge was estimated from the extrapolation of C to $v=0$, which extrapolated to $v=0$ intercept (Fig. 4(c)). From these extrapolations, a C_{outer} value of $3.69 \text{ F} \cdot \text{cm}^{-2}$ was obtained for a total charge of $4.22 \text{ F} \cdot \text{cm}^{-2}$. Therefore, C_{outer} represented 87.4% of the total charge, most of the full storable charge was rapidly accessible, which was common and necessary for high-rate performance supercapacitors.

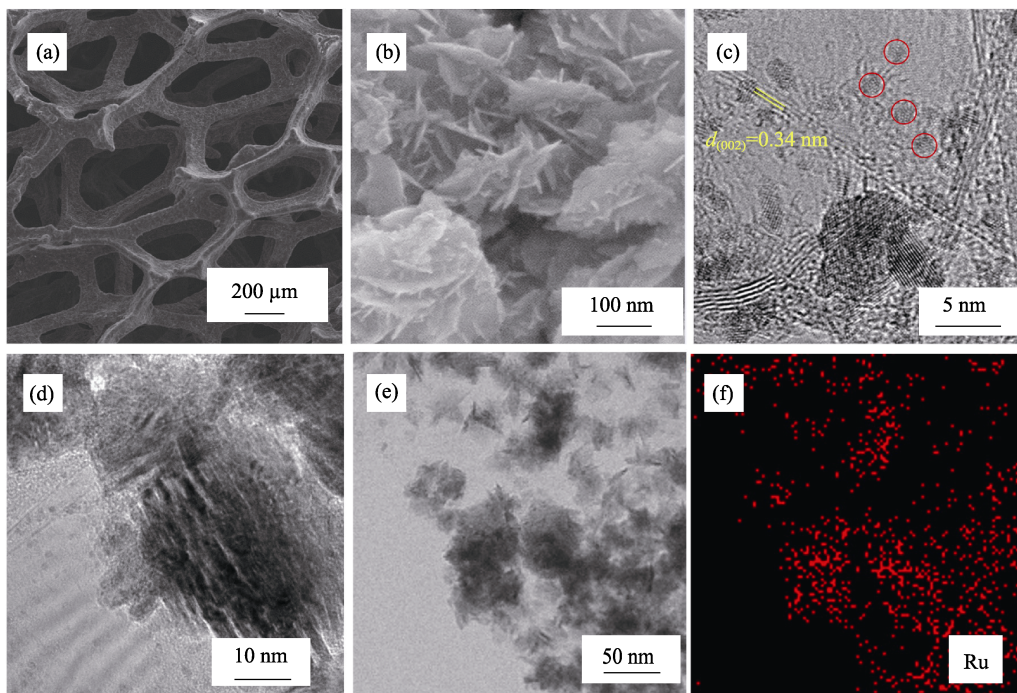


Fig. 2 FE-SEM images of (a) 3D-GR and (b) $\text{RuO}_x \cdot n\text{H}_2\text{O}$, (c-d) HRTEM images of $\text{RuO}_x \cdot n\text{H}_2\text{O}/3\text{D-GR}$, (e) TEM image of $\text{RuO}_x \cdot n\text{H}_2\text{O}$, and (f) corresponding EDS elemental mapping of (e)

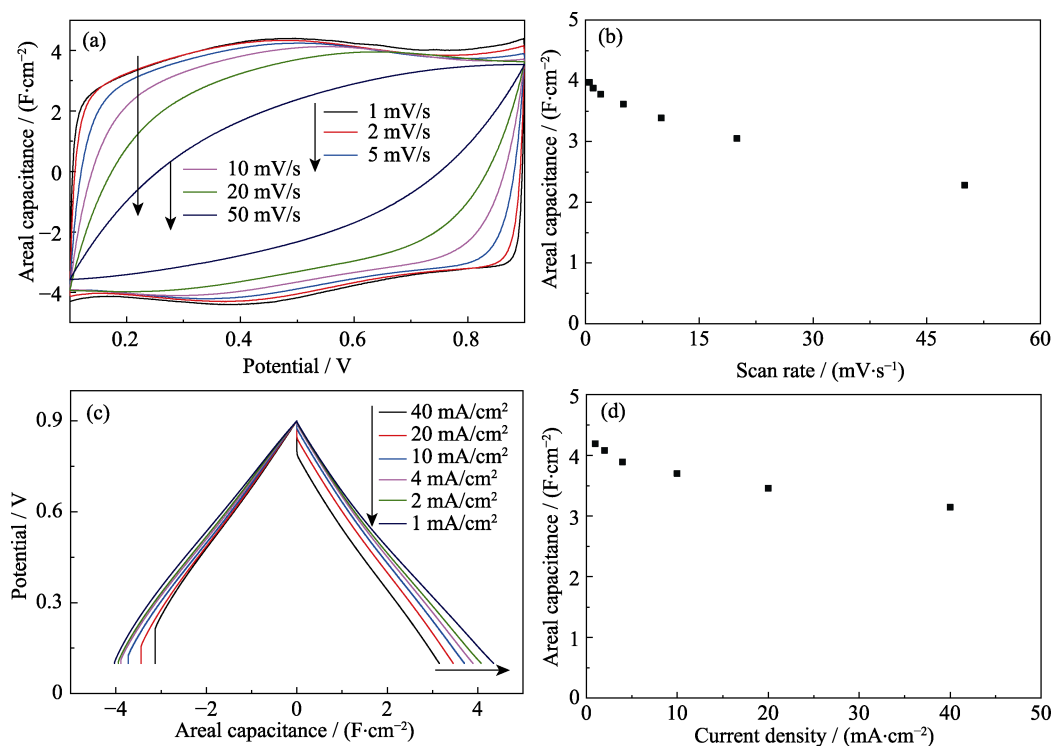


Fig. 3 (a) CV curves of RuO_x·nH₂O/3D-GR at different scan rates with current being normalized by scan rates and the area of the electrode, (b) areal capacitance calculated from CV curves vs. scan rates, (c) GCD curves of RuO_x·nH₂O/3D-GR at different current densities, and (d) areal capacitance calculated from GCD curves vs. current densities

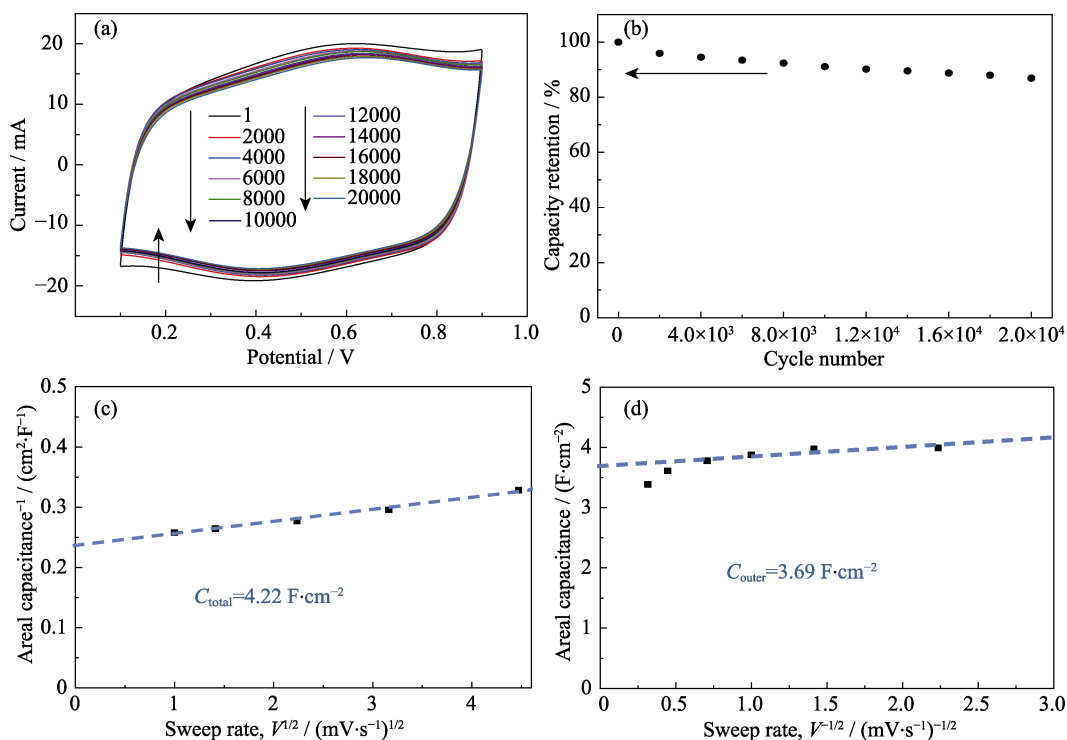


Fig. 4 (a) Different cycles of CV curves at a scan rate of 10 mV·s⁻¹, (b) calculated capacitance vs. the cycles number of CV test, determination of (c) C_{total} and (d) C_{outer} of RuO_x·nH₂O/3D-GR

All-solid-state flexible supercapacitors were fabricated by pasting RuO_x·nH₂O/3D-GR on the flexible carbon paper and using the electrolyte of H₂SO₄/PVA. CV curves (Fig. 5(a)) of this symmetric cell was rectan-

gular and rather symmetric, and the GCD curves (Fig. 5(c)) were highly linear and symmetrical, indicating excellent capacitive properties. The areal capacitance was 1.02 F·cm⁻² at the current density of 1 mA·cm⁻² and

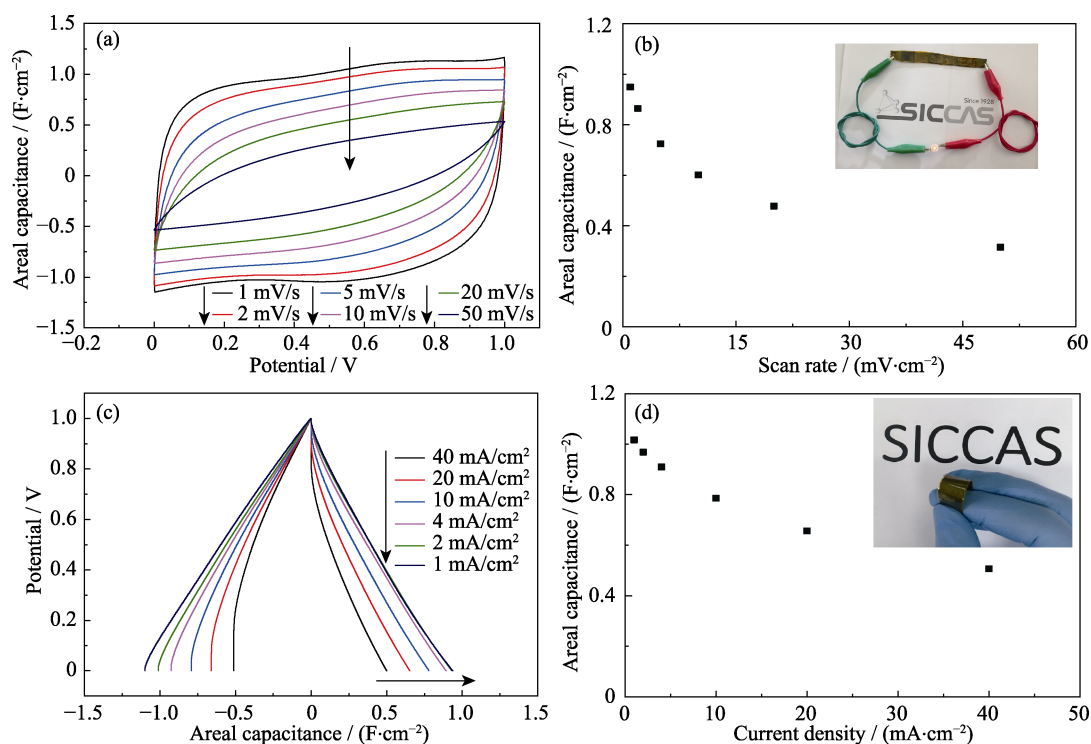


Fig. 5 Electrochemical performance of all-solid-state flexible supercapacitors

(a) CV curves of $\text{RuO}_x \cdot n\text{H}_2\text{O}/3\text{D-GR}$ at different scan rates with current being normalized by voltage scan rate v and the total area of the two electrodes; (b) Calculated capacitance from CV curves *vs.* different scan rates with inset showing the glow of red-light emitting diode (2.4 V) powered by three devices in series; (c) GCD curves of $\text{RuO}_x \cdot n\text{H}_2\text{O} /3\text{D-GR}$ at different current densities; (d) Areal capacitance calculated from GCD curves *vs.* different current densities with inset showing display of the flexible device

maintained $0.67 \text{ F} \cdot \text{cm}^{-2}$ at $20 \text{ A} \cdot \text{cm}^{-2}$, retaining 65.7% of capacitance at $1 \text{ mA} \cdot \text{cm}^{-2}$. Here, the areal capacitance was divided by the total area of the electrodes. Three in series all-solid-state flexible supercapacitors were also used to light up a red-light emitting diode (the lowest working potential was 2.4 V), as shown on the upper right of Fig. 5(b).

The energy and power density of the device was calculated from the two-electrode test. The energy density was calculated from the equation (4):

$$E = 1/2 \cdot C \cdot V^2 \quad (4)$$

and the power density from the equation $P=E/t$ (t was discharge time). In GCD test at $10 \text{ mA} \cdot \text{cm}^{-2}$, a very low IR-drop voltage (33 mV), an energy density of $0.102 \text{ mWh} \cdot \text{cm}^{-2}$ and a power density of $2.42 \text{ mW} \cdot \text{cm}^{-2}$ were achieved, which surpassed most of the state-of-the-art works.

3 Conclusions

In summary, layered $\text{RuO}_x \cdot n\text{H}_2\text{O}$ was successfully prepared *via* a cathodic electrodeposition process which was effective and easily manipulated. Due to its unique structure, an areal capacitance of $3.78 \text{ F} \cdot \text{cm}^{-2}$ was achieved at $2 \text{ mV} \cdot \text{s}^{-1}$. Besides, $\text{RuO}_x \cdot n\text{H}_2\text{O}/3\text{D-GR}$ combined with flexible carbon paper was prepared to fabricate all-solid-state flexible supercapacitors for

practical application, owning an energy density of $0.102 \text{ mWh} \cdot \text{cm}^{-2}$ and a power density of $2.42 \text{ mW} \cdot \text{cm}^{-2}$ at $10 \text{ mA} \cdot \text{cm}^{-2}$. Combining the advantages of the layered morphology and facile preparation, $\text{RuO}_x \cdot n\text{H}_2\text{O}/3\text{D-GR}$ shows promising prospect in the field of high-tech wearable equipment in which per-area performance is recognized as a critical factor.

References:

- [1] FERRIS A, GARBARINO S, GUAY D, *et al.* 3D RuO_2 microsupercapacitors with remarkable areal energy. *Advanced Materials*, 2015, **27**(42): 6625–6629.
- [2] WANG Q, WANG X, LIU B, *et al.* NiCo_2O_4 nanowire arrays supported on Ni foam for high-performance flexible all-solid-state supercapacitors. *Journal of Materials Chemistry A*, 2013, **1**(7): 2468–2473.
- [3] WALSH E D, HAN X, LACEY S D, *et al.* Dry-processed, binder-free holey graphene electrodes for supercapacitors with ultrahigh areal loadings. *ACS Applied Materials & Interfaces*, 2016, **8**(43): 29478–29485.
- [4] XIAO K, LI J W, CHEN G F, *et al.* Amorphous MnO_2 supported on 3D-Ni nanodendrites for large areal capacitance supercapacitors. *Electrochimica Acta*, 2014, **149**: 341–348.
- [5] ZHOU H, HAN G, XIAO Y, *et al.* Facile preparation of polypyrrole/graphene oxide nanocomposites with large areal capacitance using electrochemical codeposition for supercapacitors. *Journal of Power Sources*, 2014, **263**: 259–267.
- [6] QIN T, WAN Z, WANG Z, *et al.* 3D flexible O/N Co-doped gra-

- phene foams for supercapacitor electrodes with high volumetric and areal capacitances. *Journal of Power Sources*, 2016, **336**: 455–464.
- [7] YOO J J, BALAKRISHNAN K, HUANG J S, *et al.* Ultrathin planar graphene supercapacitors. *Nano Letters*, 2011, **11**(4): 1423–1427.
- [8] HUANG P, HEON M, PECH D, *et al.* Micro-supercapacitors from carbide derived carbon (CDC) films on silicon chips. *Journal of Power Sources*, 2013, **225**: 240–244.
- [9] WANG G P, ZHANG L, ZHANG J J. A review of electrode materials for electrochemical supercapacitors. *Chem. Soc. Rev.*, 2012, **41**(2): 797–828.
- [10] ICAZA J C, GUDURU R K. Electrochemical characterization of nanocrystalline RuO_2 with aqueous multivalent (Be^{2+} and Al^{3+}) sulfate electrolytes for asymmetric supercapacitors. *Journal of Alloys and Compounds*, 2018, **735**: 735–740.
- [11] SHIH Y T, LEE K Y, HUANG Y S. Characterization of iridium dioxide-carbon nanotube nanocomposites grown onto graphene for supercapacitor. *Journal of Alloys and Compounds*, 2015, **619**: 131–137.
- [12] WANG C F, LU S, CHEN H L, *et al.* One-pot synthesis and application in asymmetric supercapacitors of $\text{Mn}_3\text{O}_4/\text{RGO}$ nanocomposites. *Journal of Inorganic Materials*, 2016, **31**(6): 581–587.
- [13] ZHANG L J, GAO B, ZHANG X G. Pyrolysis preparation of nickel oxide and its electrochemical capacitance. *Journal of Inorganic Materials*, 2011, **26**(4): 398–402.
- [14] DENG W, JI X, CHEN Q, *et al.* Electrochemical capacitors utilizing transition metal oxides: an update of recent developments. *RSC Advances*, 2011, **1**(7): 1171.
- [15] YAN S, QU P, WANG H, *et al.* Synthesis of Ru/multiwalled carbon nanotubes by microemulsion for electrochemical supercapacitor. *Materials Research Bulletin*, 2008, **43**(10): 2818–2824.
- [16] YANG F, YAO J, LIU F, *et al.* Ni-Co oxides nanowire arrays grown on ordered TiO_2 nanotubes with high performance in supercapacitors. *Journal of Materials Chemistry A*, 2013, **1**(3): 594–601.
- [17] YE J S, CUI H F, LIU X, *et al.* Preparation and characterization of aligned carbon nanotube-ruthenium oxide nanocomposites for supercapacitors. *Small*, 2005, **1**(5): 560–565.
- [18] QI X Y, ZHOU Q F, CUI M W, *et al.* Capacitive performance of Zn-Ni hydroxide nano-sheet arrays on nickel foams via a mild chemical-bath deposition process. *Journal of Inorganic Materials*, 2017, **32**(4): 372–378.
- [19] WU M S, YANG C H, WANG M J. Morphological and structural studies of nanoporous nickel oxide films fabricated by anodic electrochemical deposition techniques. *Electrochimica Acta*, 2008, **54**(2): 155–161.
- [20] YANG L, CHENG S, DING Y, *et al.* Hierarchical network architectures of carbon fiber paper supported cobalt oxide nanonet for high-capacity pseudocapacitors. *Nano Letters*, 2012, **12**(1): 321–325.
- [21] SUN H, LIN M, LIANG J, *et al.* Three-dimensional holey-graphene/niobia composite architectures for ultrahigh-rate energy storage. *Science*, 2017, **356**(6338): 599–604.
- [22] CHEN Y, ZHANG X, ZHANG D, *et al.* One-pot hydrothermal synthesis of ruthenium oxide nanodots on reduced graphene oxide sheets for supercapacitors. *Journal of Alloys and Compounds*, 2012, **511**(1): 251–256.
- [23] WANG Z, MA C, WANG H, *et al.* Facile synthesized Fe_2O_3 -graphene nanocomposite as novel electrode materials for supercapacitors with high performance. *Journal of Alloys and Compounds*, 2013, **552**: 486–491.
- [24] XU J, DING W, ZHAO W, *et al.* In situ growth enabling ideal graphene encapsulation upon mesocrystalline MTiO_3 ($\text{M} = \text{Ni}, \text{Co}, \text{Fe}$) nanorods for stable lithium storage. *ACS Energy Letters*, 2017, **2**(3): 659–663.
- [25] ARDIZZONE S, FREGONARA G, TRASATTI S. Inner and outer active surface of RuO_2 electrodes. *Electrochimica Acta*, 1990, **35**(1): 263–267.
- [26] LIN T, CHEN I. W, LIU F, *et al.* Nitrogen-doped mesoporous carbon of extraordinary capacitance for electrochemical energy storage. *Science*, 2015, **350**(6267): 1508–1513.

基于三维石墨烯衬底的纳米片状水合氧化钌：电化学沉积制备以及柔性超级电容器储能应用

王 远^{1,2}, 林 杰^{1,2}, 常 郑¹, 林天全¹, 钱 猛^{1,2}, 黄富强^{1,3}

(1. 中国科学院 上海硅酸盐研究所, 高性能陶瓷和超微结构国家重点实验室, 上海 200050; 2. 中国科学院大学, 北京 100049; 3. 北京大学 化学与分子工程学院, 北京分子科学国家实验室, 稀土材料化学及应用国家重点实验室, 北京 100871)

摘 要: 可穿戴设备的快速发展刺激了对柔性高容量储能设备的迫切需求。本工作采用一种简单的无粘结剂阴极电沉积方法将纳米片状 $\text{RuO}_x \cdot n\text{H}_2\text{O}$ 沉积固定在三维石墨烯骨架上, 以提高 $\text{RuO}_x \cdot n\text{H}_2\text{O}$ 的利用效率, 实现了更优良的电极导电性, 并缩短了质子和电子的扩散传输路径。在 $2 \text{ mV} \cdot \text{s}^{-1}$ 时, 它的面容量高达 $3.78 \text{ F} \cdot \text{cm}^{-2}$, 主要归因于材料的纳米层状结构有利于电解质进入活性物质 $\text{RuO}_x \cdot n\text{H}_2\text{O}$ 的内部。另外, 以这种电极材料制备得到的全固态柔性超级电容器, 在 $10 \text{ mA} \cdot \text{cm}^{-2}$ 的电流密度下, 能量密度达到 $0.1 \text{ mWh} \cdot \text{cm}^{-2}$, 功率密度达到 $2.4 \text{ mW} \cdot \text{cm}^{-2}$, 超过大部分文献报道。

关 键 词: 纳米片状 $\text{RuO}_x \cdot n\text{H}_2\text{O}$; 电化学沉积; 超级电容器

中图分类号: O782 文献标识码: A

Supporting information:

Electrodeposited Nanoflakes of $\text{RuO}_x \cdot n\text{H}_2\text{O}$ on Three-dimensional Graphene for Flexible Supercapacitors

WANG Yuan^{1,2}, LIN Jie^{1,2}, CHANG Zheng¹, LIN Tian-Quan¹, QIAN Meng^{1,2}, HUANG Fu-Qiang^{2,3}

(1. State Key Laboratory of High Performance Ceramics and Superfine Microstructure, Shanghai Institute of Ceramics, Chinese Academy of Sciences, Shanghai 200050, China; 2. University of Chinese Academy of Sciences, Beijing 100049, China; 3. State Key Laboratory of Rare Earth Materials Chemistry and Applications and Beijing National Laboratory for Molecular Sciences, College of Chemistry and Molecular Engineering, Peking University, Beijing 100871, China)

Obviously, the capacitances increased dramatically after the deposition of $\text{RuO}_x \cdot n\text{H}_2\text{O}$ (Fig. S1(a) and Fig. S1(b)). The capacitance of 3D-GR only contained 2.77% of the whole capacitance in the three-electrode setup which is half-cell test, while it contained 2.63% in the two-electrode setup which is full-cell test. The capacitance of $\text{RuO}_x \cdot n\text{H}_2\text{O}/3\text{D-GR}$ mainly came from $\text{RuO}_x \cdot n\text{H}_2\text{O}$.

EIS was conducted to investigate the ion transport behavior and electrical resistance of $\text{RuO}_x \cdot n\text{H}_2\text{O}/3\text{D-GR}$ electrodes. As shown in Fig. S2, the x -intercept of the Nyquist plot was 1.7Ω , indicating the internal resistance (R_s) of $\text{RuO}_x \cdot n\text{H}_2\text{O}/3\text{D-GR}$ electrodes were 1.7Ω . The small semicircle at high frequency which was the charge transfer resistance also reached a low value of 0.6Ω . The equivalent series resistance was 2.3Ω , which was the sum of internal resistance and charge transfer resistance. The vertical line at low frequency demonstrated its good electrochemical capacitive property. Perfect electrochemical capacitive performance of $\text{RuO}_x \cdot n\text{H}_2\text{O}/3\text{D-GR}$ can be seen from these results.

X-ray photoelectron spectroscopy (XPS) was performed to confirm the valence states of deposited ruthenium. As shown in Fig. S3(a), fitting was undertaken by considering different oxidation states of Ru. The lowest energy state at 280.0 eV was assigned to the metallic ruthenium Ru (0), and the higher binding energies were assigned to

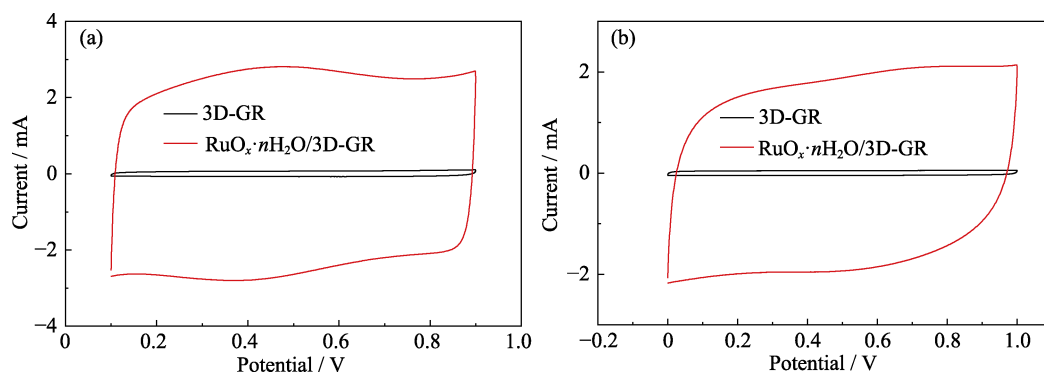


Fig. S1 CV curves of $\text{RuO}_x \cdot n\text{H}_2\text{O}/3\text{D-GR}$ and 3D-GR at a scan rate of $2 \text{ mV} \cdot \text{s}^{-1}$ in $1 \text{ mol/L H}_2\text{SO}_4$ (a) three-electrode setup; (b) two-electrode setup

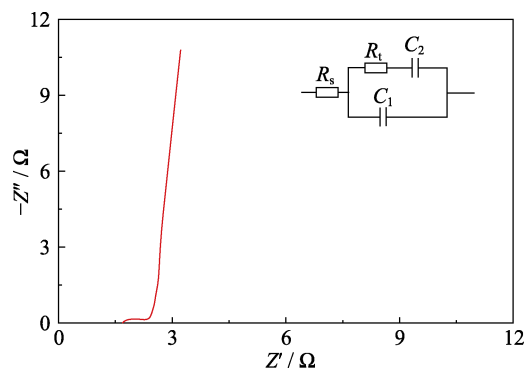


Fig. S2 EIS curve of the $\text{RuO}_x \cdot n\text{H}_2\text{O}/3\text{D-GR}$ electrode (inset: the equivalent circuit of EIS)

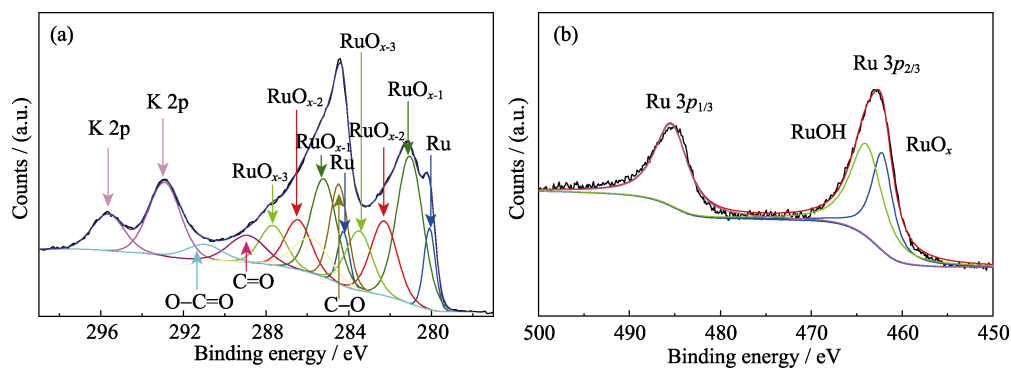


Fig. S3 High-resolution XPS spectra of $\text{RuO}_x \cdot n\text{H}_2\text{O}/3\text{D-GR}$ (a) of Ru 3d3/2 and Ru 3d5/2; (b) High-resolution XPS spectra of Ru 3p3/2

oxidation state of ruthenium^[1], either through surface oxidation in the process of deposition, or during the annealing process. As Fig. S3(b) shown, the Ru 3p3/2 peak was deconvoluted into two peaks, which were ascribed to RuO_x (462.2 eV) and RuOH (464.1 eV)^[2]. There existed different oxidation states of Ru on 3D-GR can be concluded from the XPS spectra.

References:

- [1] OPPEDISANO, D, JONES, L, JUNK, T, *et al.* Ruthenium electrodeposition from aqueous solution at high cathodic overpotential. *Journal of the Electrochemical Society*, 2014, **161**(10): D489–D494.
- [2] WANG W, GUO S, LEE I, *et al.* Hydrous ruthenium oxide nanoparticles anchored to graphene and carbon nanotube hybrid foam for supercapacitors. *Sci. Rep.*, 2014, **4**: 4452–1–9.